# ChemComm

Accepted Manuscript


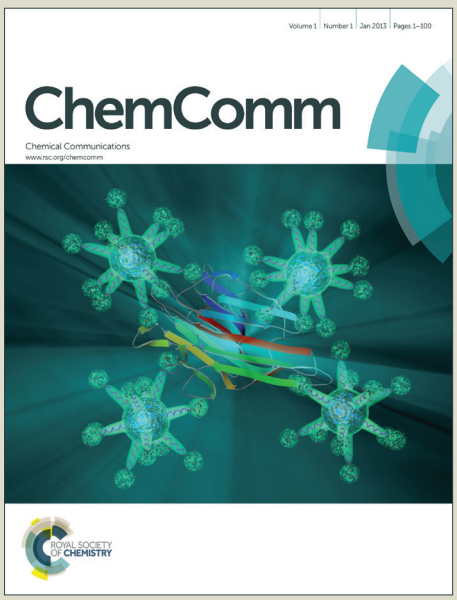





ROYAL SOCIETY OF CHEMISTRY

www.rsc.org/chemcomm

**Graphical abstract**

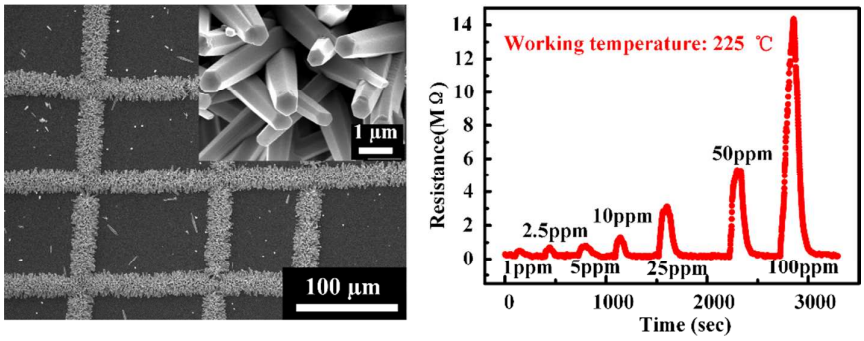


Micropatterned ZnO nanorods array fabricated by mechanoelectrospinning and hydrothermal growth mothed exhibited excellent sensitivity response to $NO_2$.

Journal Name

RSCPublishing

COMMUNICATION

# Patterned ZnO nanorod array/gas sensor by mechanoelectrospinning-assisted selective growth†

Cite this: DOI: 10.1039/xoxxoooooox

Xiaomei Wang,[a] Fazhe Sun,[b] Yongan Huang,*[a] Yongqing Duan,[a] and Zhouping Yin,*[a]

Received ooth January 2012,
Accepted ooth January 2012

DOI: 10.1039/xoxxoooooox

www.rsc.org/

**Micropatterned ZnO nanorod arrays were fabricated by mechanoelectrospinning-assisted direct-writing process and hydrothermal growth process, and utilized as gas sensor that exhibited excellent Ohmic behavior and sensitivity response to oxidizing gas $NO_2$ at low concentrations (1-100 ppm).**

Zinc oxide (ZnO) is a typical n-type direct wide band gap (3.37 eV) and large excitation binding energy (60 MeV) semiconductor, and it plays an important role in many fields ranging from optoelectronics to energy conversion, photocatalysis, photodectors, and nanosensors[1-3]. One-dimensional ZnO nanostructure has attracted much attention owing to its extensive applications in light-emitting diodes[4, 5], thin film transistors[6], field-effect transistors[3, 7], chemical sensors[7], piezoelectric sensors[8] and solar cells[9].

The synthesis of ZnO nanostructures has been carried out using various methods, such as aqueous electrodeposition[10], thermal evaporation and condensation[11], physical/chemical vapor deposition[4, 12], solvothermal method[13] and hydrothermal method[14]. Among these methods, the hydrothermal method has been considered as an excellent procedure for the preparation of crystalline nanomaterials due to its low-cost, low temperature, simple process control, environment-friendly nature. In nanodevices, it is significant to realize patterned and aligned ZnO nanorods, representing more integrated applications. Instead of randomly distributed nanorods on a substrate, an effective method is to selectively grow nanostructures directly desired areas of substrate. Generally, the technique utilized to achieve a site-specific growth of ZnO nanorods involves micropatterning of precursor and selective growth. It is hard to find suitable etching conditions in ceramic thin films to obtain patterned ZnO nanorods. Various methods for ZnO micropattern preparation have been reported, such as ink-jet printing[15-17], self-assembled monolayer[18], microcontact printing[19], nanoimprint lithography[20], pulsed laser deposition[21] and photolithography[22]. However, these approaches are limited by high temperature treatment, high vacuum system, lithography or complication of process and the need of a mask or a mold.

This work presents a mechanoelectrospinning (MES)-assisted selective growth technique to fabricate patterned ZnO nanorod array/gas sensor. It utilizes a MES direct-writing method[23, 24] to deposit the fiber-lattices of precursor. MES adopts a short nozzle-to-substrate distance to improve positioning of the electrospun fibers of ZnAc precursor. The diameter and position of the deposited fiber can be controlled over large-area substrate in a direct, continuous manner. This method can fabricate orderly nanofibers continuously with a high local positioning accuracy. The combination of MES method and low-temperature hydrothermal method is presented for selectively growing ZnO nanorods. By tuning the printing conditions and the hydrothermal reaction time, the aligned arrays of ZnO nanorod with tunable spacing/diameter, uniform morphology and good crystal quality can be achieved. Finally, the ZnO nanorod array on alumina substrate with interdigital electrode is exposed to oxidizing gas $NO_2$[25] at low concentrations at 225 ºC. It is indicated that ZnO sample has a good Ohmic behavior and high response to $NO_2$. Patterned of ZnO parallel array is easier integrated with other functional materials or electronic diveces than ZnO film of randomly distributed nanorods for gas sensing. The presented technique can fabricate patterned ZnO nanorod array/gas sensor in a direct, low-cost, low-temperature, template-free, and highly controllable manner.

The experimental setup of MES is shown in Figure 1(a). MES process needs two electrodes: 1) a stainless steel nozzle is adopted as one electrode, connecting with a high voltage DC power supplier and a syringe pump; and 2) another electrode is the ground collector which is fixed on the X-Y moving stage. The substrate is mounted on the ground collector underneath the nozzle. The nozzle-to-substrate distance maintains 2-5 mm, which is much shorter than conventional electrospinning. A high-speed camera is used to observe the dynamic process of the jet.

*a State Key Laboratory of Digital Manufacturing Equipment and Technology, Huazhong University of Science and Technology, Wuhan 430074, China*

*b Analysis Testing Center, Shandong University of Technology, Zibo 255100, China*

*E-mail: yahuang@hust.edu.cn, and yinzhp@mail.hust.edu.cn.*

† Electronic Supplementary Information (ESI) available: Materials and equipments, ZnAc seed layer synthesis and ZnO nanorod selective growth, characterization. See DOI: 10.1039/c000000x/

An aqueous solution containing zinc acetate (ZnAc) and polyethylene oxide (PEO) is fabricated by magnetic stirring. Initially, the nozzle shown in Figure 1(a) is filled with ZnAc precursor solution. When 1.5-2.75 kV voltage and 450-900 nl/min flow rate are applied, the solution is sucked out from the needle, attaches to the nozzle orifice, and forms Taylor cone at the apex of the nozzle (Figure 1(a) I). Then the applied voltage increases gradually up to the onset voltage. As the electrostatic force is sufficient to overcome the surface tension of the sucked solution, a thin jet ejects from the apex of the Taylor cone, and forms a fiber between the nozzle and the substrate (Figure 1(a) II). Then, the applied voltage is reduced gradually and appropriately just to keep the jet stable. The liquid jet undergoes extensive stretching forming linear fibers on the substrate orderly by the mechanical drawing force in one direction (Figure 1(a) III). Meanwhile, the jet diameter becomes controllable due to the mechanical drawing force resulted from the digitally controllable high-speed motion.[26, 27]

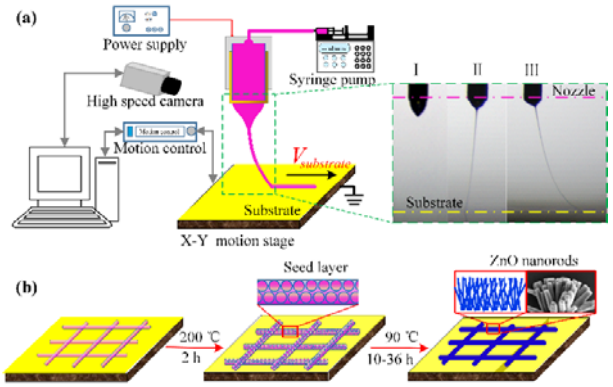


Figure 1 (a) Schematic diagram of MES setup. I, II and III are the images of the jet in deferent stages indicated by dashed line box. (b) Growth process of the directly patterned ZnO nanorod array.

Hydrothermal growth ZnO nanorod array was carried out in three steps. An aqueous solution containing PEO making electrospinning easier and ZnAc was direct-written on Si substrate by MES. Then the obtained samples were annealed at 200 ºC for 2 hours to form ZnAc nanoparticles nuclei and to ensure the seed particle adhesion to substrate formed the seed layer. Finally, direct patterned ZnO nanorod arrays were selectively grown from ZnAc nanoparticle nuclei through hydrothermal growth (see ESI†). The whole experimental process schematics was shown in Figure 1(b).

To fabricate the two-dimensional orthogonal microstructure of a large-area, well-defined ZnAc array (Figure 2(a)), parallel array of ZnAc and PEO was first direct-written along one direction, then along the perpendicular direction. The samples of the parallel and orthogonal array of ZnAc and PEO were annealed to fabricate ZnAc nanoparticle nuclei as seed layer. ZnO nanorod array was grown by subsequent selective hydrothermal growth. Figure 2(b) and (c) show the field emission scanning electron microscope (SEM) images of parallel and orthogonal array of ZnO nanorods respectively. High-density, radially grown, flower-type structures are shown in the insets of Figure 2(b) and (c). The width of flower-like structure is about 20 μm, and the distributions are uniform. Additionally, the ZnO nanorods originated from the center of the flower are randomly grown in all directions. In fact, the central part of the flower-shape structure corresponding to ZnO seed particle nuclei formed on the substrate provides a root for the growth of the ZnO nanorods.

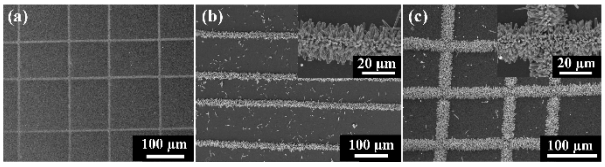


Figure 2 (a) Low magnified SEM image of patterned ZnAc-PEO arrays on Si substrate by MES; ZnO nanorod array subsequent selective hydrothermal growth (b) parallel array, (c) orthogonal array, the insets are high magnification SEM images of parallel array and orthogonal array respectively.

Typical X-ray diffraction (XRD) patterns of ZnO nanorods are shown in Figure 3(a). All the diffraction peaks are well indexed to the standard diffraction pattern of hexagonal phase ZnO with lattice constants of a = 0.3249 nm and c = 0.5206 nm (JCPDS card no. 36-1451). The grown structure is c-axis oriented. In addition, in comparison with the standard XRD pattern, the intensity ratio of (002) to (101) diffraction peak which is the usual maximum reflection increases significantly, indicating that (001) is the relatively preferred growth direction of the structure, the orientation of ZnO nanorod is further improved. Moreover, there is a Si peak at 28.37º owing to the existence of the Si substrate. The sharp diffraction peaks representing narrow spectral width of the obtained ZnO peaks indicate that the as-grown nanorods are highly crystalline with less impurities.

Individual ZnO nanorod is faceted as indicated in Figure 3(b, c). ZnO nanorod is highly crystalline, with a lattice spacing of about 0.26 nm, corresponding to the distance between adjacent (002) lattice planes. The selected-area electron diffraction (SAED) pattern confirms that ZnO nanorod has a single crystalline structure and its growth direction is along c-axis orientation, which corresponds to the (001) direction. It is in accordance with low index crystallographic faces growth. In addition, the high-resolution transmission electron microscope (HR-TEM) image clearly shows an absence of stacking defects in the crystalline structure, which suggests that the crystals of individual rods are of good quality.

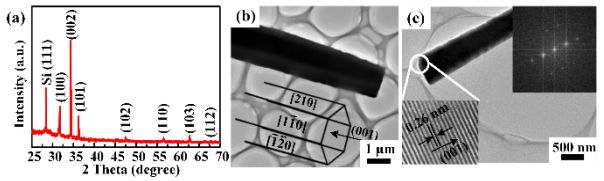


Figure 3 (a) XRD patterns of ZnO nanorods growing for 12 h. (b, c) TEM image of single nanorods growing for 12 h, the bottom left inset in (c) is HR-TEM image of the area indicated by the white circle, the upper right inset image represents SAED pattern of ZnO.

Figure 4 shows the SEM images of ZnO nanorods sample growing at different positions of the reaction kettle, whose interlining is teflon-bottle. ZnO nanorods grow at unwanted areas in Figure 4(a). During the growth reaction, ZnO powders are generated inside of the growth solution at the beginning of the growth, and then deposit onto the sample substrate as ZnO growth seed, which continue to grow ZnO nanorods. Temperature unevenness of the growth solution produces directional flow solution, and the patterned nanoparticle seeds move to the unpatterned (unseeded) adjacent substrate region due to the strong convective flow, which grow ZnO nanorods similarly. Based on above two factors, growth of ZnO nanorods at the bottom of the reaction kettle is undesirable. Secondary there is no ZnO nanopowder settlement to the sample at the sidewall in the reaction kettle, but the directional flow generated by the effect of the uneven temperature is still there, so the sample (Figure 4(b)) is better than the sample at the bottom. Invert the sample at the top of the teflon-bottle kettle and let the seeded side of the substrate upside-down immersed



 

in the growth solution. There will be no above two factors, ZnO nanorods grow just at wanted areas (Figure 4(c)). ZnO nanorod array is greatly improved. So the position and the orientation of the ZnO precursor sample in the reactor play an important role in the growth of ZnO nanorod array. The sample inverted on the top of the teflon-bottle is the ideal position and orientation, and the ZnO nanorods pattern is optimized.

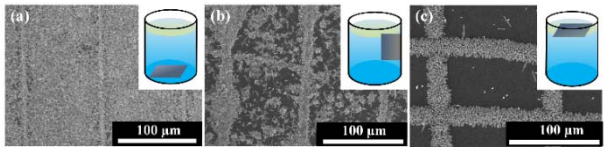


Figure 4 SEM images of ZnO nanorods growing sample (a) at the bottom, (b) at the sidewall and (c) upside-down at the top of teflon-bottle. The insets are the corresponding schematic diagrams of the sample position located.

At different growth stages, the lateral and axial surface growths are found to have different relative growth rates. During the beginning 10 hours (h), axial growth is more significant than lateral growth, as shown in Figure 5(a, b). Due to the anisotropic crystal property, the velocities of growth in different directions under hydrothermal condition are $V_{[0001]} > V_{[0110]} > V_{[1000]}$[28]. The diameter of individual ZnO nanorod decreases gradually from the bottom to the top exhibiting tower-like shape. The initial seed layer can serve as heterogeneous nucleation sites and initiate a layer-by-layer growth along the c-axis, which results in the formation of tower-like nanorod[29]. Moreover, the side and top surfaces of nanorods are very smooth and clean. When the growth time exceeds 10 h, lateral growth is more significant than axial growth. The nanorods are obviously increased in diameter but are always about 5-15 μm in length (Figure 5(c-f)) when growth time is from10 to 36 h. The length of ZnO nanorods is almost independent of time, indicating little axial growth. Side and most of top surfaces of the ZnO nanorods are very smooth and clean, while few top surfaces are observed protrusions but smooth (Figure 5(d)) due to the beginning of erosion by the growth solution . During the period of 36 h (Figure 5(e)), ZnO nanorods diameter increases slower with growth time of36 h than that of ZnO nanorods growing for 12 h, and the top of the nanorods is subjected to erosion by the growth solution, and the shape becomes irregular (Figure 5(f)).

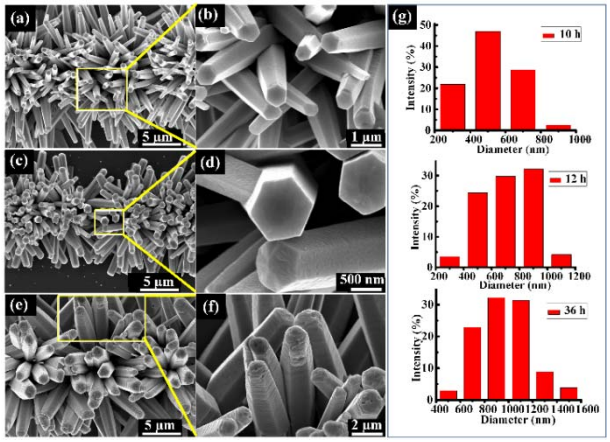


Figure 5 SEM images of ZnO nanorods growing upside-down in the teflon-bottle at 90 ℃ for (a, b) 10 h; (c, d) 12 h; (e, f) 36 h. (g) Histograms of ZnO nanorods top diameter distribution with different growth time.

The top diameter distributions of ZnO nanorods are presented in Figure 5(g). More than 160 nanorods are tested in order to determine the diameter distribution. The quantitative analysis shows that the regions of top diameter distributions are enlarged and the average top diameters increase with increasing the growth time from 10 h to 36 h. When the growth time is 10 h, the ZnO nanorods obtained have uniform diameters between 200-1000 nm, and the average top diameter is 520 nm with a standard deviation of 153 nm. The diameters of nanarods for longer growth time (12 h) distribute in the range of 200-1200 nm with the average top diameter of 728 nm (±183 nm). However, the region of distribution with growth time of 36 h ranges from 400 to 1600 nm, and the average top diameter is 962 nm (±214 nm).

Adjusting the process parameters, we have prepared gas sensor of ZnO parallel array on alumina substrate with Ag interdigital electrode (Ag IDT), which is shown in Figure 6(a). The current-voltage (I-V) characteristic (Figure 6(b)) indicates that the electrical current is linearly proportional to the intensity of applied bias voltage (−10-10 V), which evidents that ZnO sample has Ohmic behavior rather than diode-like behaviour. This is beneficial for gas sensing properties because the sensitivity of a gas sensor can be maximized when the metal-semiconductor junction is Ohmic behavior or has a negligible junction resistance.

ZnO sample is not suitable for using as $NO_2$ sensor at room temperature[30], but has good sensitivity to $NO_2$ at 225 ºC. Figure 6(c) shows dynamic responses of ZnO sample to nitrogen dioxide ($NO_2$) gas at various concentrations from 1 to100 ppm at 225 ºC. The resistance increases instantaneously to a maximum resistance, which is maintained at the maximum resistance upon exposure to $NO_2$ and recovered completely to the initial value upon the removal of $NO_2$. The response of ZnO sample to $NO_2$ gas is stable and reproducible for repeat test.

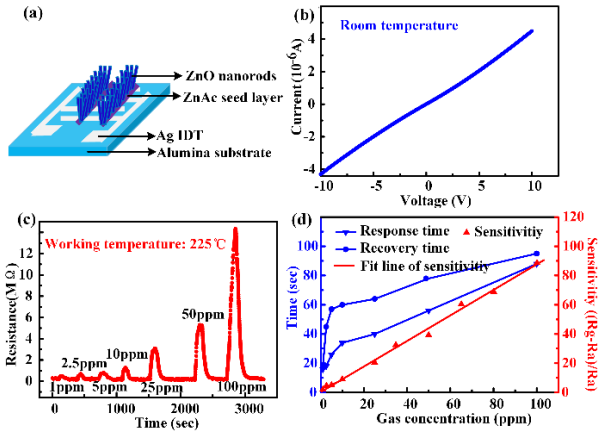


Figure 6 (a) Schematics of ZnO gas sensor. (b) Room-temperature I-V characteristic of a ZnO-nanorod gas sensor in air atmosphere. (c) Dynamic responses of ZnO sample to $NO_2$ gas. (d) Variation of sensitivities, response and recovery time of ZnO sample to different concentrations of $NO_2$.

The corresponding sensitivities(S) are commonly given by equation: S=(Rg-Ra)/Ra, where Rg is the resistance of sample under $NO_2$ atmosphere and Ra is sample resistance under air atmosphere. Figure 6(d) shows the S of ZnO sample versus $NO_2$ concentrations in the range of 1-100ppm. The data of S has been fitted by least squares fitting. It is clearly seen that S increases from 1 to 88 with increasing concentration, and an approximately linear increase relationship between the corresponding sensitivities and $NO_2$ concentrations is observed for ZnO sample in the measured concentration. The response time is defined as the time taken by the sensor to attain 90% of the maximum increase in resistance on exposure of target gas and recovery time as the time to get back to 90% of the maximum resistance when exposed to clean air. The variations of response and

recovery time with different concentrations of $NO_2$ are represented in Figure 6(d). It is observed that the response and recovery time are both increased with respect to $NO_2$ concentration, and the increases slow down gradually when the gas concentrations increase. The response time increases from 16 s to 88 s while recovery time is relatively ranging from 18 to 95 s with increasing $NO_2$ concentration from 1 to 100 ppm. This is expected for a reasonable sensor to recover in a short period of time to be prepared.

## Conclusions

The paper presents selective growing ZnO nanorods by a combination of MES and low-temperature hydrothermal synthesis method which is demonstrated to be an excellent method for patterned ZnO nanostructure array fabrication. By varying the printing conditions and the hydrothermal reaction time, the structure of ZnO nanorod array can be fabricated in a low cost, low-temperature, template-free, environment friendly, and highly controllable manner. High-density, radially grown, flower-type structures are clearly observed, and the distributions of these tower-like nanorods are uniform. I-V characteristics and sensing measurements indicate that the ZnO sample has a good Ohmic behavior and high response to oxidizing gas $NO_2$ at low concentrations (1-100 ppm) at 225 ºC. Both response and recovery are very fast for ZnO sample exposed to $NO_2$ and clean air respectively. These findings introduce new opportunities to obtain patterned nanostructure materials used in gas sensing. Similar methods can be applied to fabricate almost any patterned shapes and any seed-growing nanostructure materials.

The authors acknowledge supports from the National Natural Science Foundation of China (51175209, 51035002) and the Fundamental Research Funds for the Central Universities (2013YQ048).

## Notes and references

1 D. Chandra, S. Mridha, D. Basak and A. Bhaumik, *Chem. Commun.* , 2009, 2384-2386.
2 M. Willander, O. Nur, Q. X. Zhao, L. L. Yang, M. Lorenz, B. Q. Cao, J. Z. Perez, C. Czekalla, G. Zimmermann, M. Grundmann, A. Bakin, A. Behrends, M. Al-Suleiman, A. El-Shaer, A. C. Mofor, B. Postels, A. Waag, N. Boukos, A. Travlos, H. S. Kwack, J. Guinard and D. L. Dang, *Nanotechnology*, 2009, **20**.
3 R. Zou, G. He, K. Xu, Q. Liu, Z. Zhang and J. Hu, *J. Mater. Chem. A*, 2013, **1**, 8445-8452.
4 W. Z. Xu, Z. Z. Ye, Y. J. Zeng, L. P. Zhu, B. H. Zhao, L. Jiang, J. G. Lu, H. P. He and S. B. Zhang, *Appl. Phys. Lett.* , 2006, **88**, 173506-173503.
5 L. C. Chen, C. H. Tien, Y. M. Luo and C. S. Mu, *Thin Solid Films* 2011, **519**, 2516-2519.
6 E. Lee, J. Ko, K. H. Lim, K. Kim, S. Y. Park, J. M. Myoung and Y. S. Kim, *Adv. Funct. Mater.* , 2014, **24**, 4689-4697.
7 R. Ahmad, N. Tripathy, D. U. J. Jung and Y.-B. Hahn, *Chem. Commun.* , 2014, **50**, 1890-1893.
8 G. Kiriakidis, I. Kortidis, S. D. Cronin, N. J. Morris, D. R. Cairns and K. A. Sierros, *Thin Solid Films* 2014, **555**, 68-75.
9 S. Kim, C. H. Kim, S. K. Lee, J. H. Jeong, J. Lee, S. H. Jin, W. S. Shin, C. E. Song, J. H. Choi and J. R. Jeong, *Chem. Commun.* , 2013, **49**, 6033-6035.
10 F. Xu, Y. Lu, L. Sun and L. Zhi, *Chem. Commun.* , 2010, **46**, 3191-3193.
11 Y. C. Chen, C. H. Tu, Y. F. Lai, K. Y. Hsu and C. P. Liu, *J. Alloys Compd.* , 2013, **554**, 115-121.
12 L. Wang, X. Zhang, S. Zhao, G. Zhou, Y. Zhou and J. Qi, *Appl. Phys. Lett.* , 2005, **86**, 024108-024103.
13 M. Wang, B. Zhao, S. Xu, L. Lin, S. Liu and D. He, *Chem. Commun.* , 2014, **50**, 930-932.
14 D. Polsongkram, P. Chamninok, S. Pukird, L. Chow, O. Lupan, G. Chai, H. Khallaf, S. Park and A. Schulte, *Physica B* 2008, **403**, 3713-3717.
15 C. J. Chang, S. Hung, C. K. Lin, C. Y. Chen and E. H. Kuo, *Thin Solid Films* 2010, **519**, 1693-1698.
16 M. Barret, S. Sanaur and P. Collot, *Org. Electron.* , 2008, **9**, 1093-1100.
17 L. V. Gambuzza, Ph.D. Thesis, Università degli Studi di CATANIA, 2014.
18 H. Shao, X. Qian and B. Huang, *Mater. Sci. Semicond. Process.* , 2007, **10**, 68-76.
19 H. W. Kang, J. Yeo, J. O. Hwang, S. Hong, P. Lee, S. Y. Han, J. H. Lee, Y. S. Rho, S. O. Kim, S. H. Ko and H. J. Sung, *J. Phys. Chem. C* 2011, **115**, 11435-11441.
20 K. S. Han, S. H. Hong, K. I. Kim, J. Y. Cho, K. W. Choi and H. Lee, *Nanotechnology*, 2013, **24**, 045304.
21 A. N. Hattori and H. Tanaka, Annual Conference on Oxide-Based Materials and Devices V, San Francisco, CA, 2014.
22 J. Yeo, S. Hong, M. Wanit, H. W. Kang, D. Lee, C. P. Grigoropoulos, H. J. Sung and S. H. Ko, *Adv. Funct. Mater.* , 2013, **23**, 3316-3323.
23 N. Bu, Y. Huang, X. Wang and Z. Yin, *Mater. Manuf. Processes* 2012, **27**, 1318-1323.
24 Y. Huang, X. Wang, Y. Duan, N. Bu and Z. Yin, *Soft Matter*, 2012, **8**, 8302-8311.
25 H. Liu, M. Li, O. Voznyy, L. Hu, Q. Fu, D. Zhou, Z. Xia, E. H. Sargent and J. Tang, *Adv. Mater.* , 2014, **26**, 2718-2724.
26 Y. Duan, Y. Huang, Z. Yin, N. Bu and W. Dong, *Nanoscale*, 2014, **6**, 3289-3295.
27 Y. Huang, Y. Duan, Y. Ding, N. Bu, Y. Pan, N. Lu and Z. Yin, *Sci. Rep.*, 2014, **4**.
28 H. Yang, Y. Song, L. Li, J. Ma, D. Chen, S. Mai and H. Zhao, *Crystal Growth & Design*, 2008, **8**, 1039-1043.
29 F. Sun, X. Qiao, F. Tan, W. Wang and X. Qiu, *Appl. Surf. Sci.* , 2012, **263**, 704-711.
30 S. Özturk, N. Kilinc and Z. Z. Ozturk, *J. Alloys Compd.* , 2013, **581**, 196-201.



 